Available online at www.sciencedirect.com
SCIENCE DIRECT
Polymer 46 (2005) 3043–3055
polymer
www.elsevier.com/locate/polymer

Structure and thermal stability of polyethylene nanolayers

T.E. Bernal-Lara[1], R.Y.F. Liu[2], A. Hiltner*, E. Baer

Department of Macromolecular Science and Engineering, Center for Applied Polymer Research, Case Western Reserve University, Cleveland, OH 44106-7202, USA

Received 6 October 2004; received in revised form 21 December 2004; accepted 28 January 2005
Available online 14 March 2005

Abstract

Confinement of the crystallizable polymer chain to the lamellar size scale is expected to affect nucleation and growth habit to the extent that new crystalline structures might be created. In this study, films with hundreds of extremely thin layers of high density polyethylene (HDPE) sandwiched between thicker polystyrene (PS) layers were fabricated by 'forced assembly' using layer multiplying coextrusion. Thermal analysis showed that as the HDPE layers became thinner, the crystallinity decreased from about 60% to almost 30%. Decreased crystallinity was accompanied by a change in morphology from banded discoids in HDPE microlayers (>100 nm) to long bundles of edge-on lamellae in HDPE nanolayers (<100 nm) as shown by atomic force microscopy and wide angle X-ray diffraction. Changes in crystallinity and crystalline morphology were responsible for an increase in oxygen permeability of the HDPE layer by a factor of 3 as the layer thickness decreased from 1.1 μm to 20 nm. It is inherent to the concept of forced assembly that nanolayers may not be stable when they are heated into the melt state. Heating films above the melting temperature of HDPE resulted in fractionated crystallization as indicated by two crystallization exotherms in thermograms. The lower temperature exotherm at 80 °C was identified with homogeneous nucleation. The droplets responsible for fractionated crystallization resulted from instability and breakup of the layers when they were taken into the melt. The number of nanodroplets formed by breakup of nanolayers was large enough that the majority did not contain an active heterogeneity and crystallization occurred primarily by homogeneous nucleation.

Keywords: Polyethylene; Nanolayer; Fractionated crystallization

1. Introduction

The application of polymers in the rapidly developing nanotechnology and microelectronics fields often requires design and fabrication of ultrathin and sometimes highly constrained polymer layers. Evidence that polymer properties such as glass transition temperature, toughness, permeability, stability and crystallizability are significantly altered as bulk polymers become thinner and more 2-dimensional, [1–7] drives the need for fundamental understanding of size-scale dependent properties.

Studies of 2-dimensional crystallization usually employ thin films with a free surface. Crystallization under conditions of spatial confinement is more difficult to access experimentally. The minute quantity of material in confined ultrathin films challenges conventional techniques of polymer structure-property characterization. Although the amount of material in a single layer is very small, the number of layers can be multiplied many-fold by layer-multiplying coextrusion. In contrast to the well-known concept of self-assembly [8], layer-multiplying coextrusion uses forced assembly to create thousands of alternating layers of two polymers [9–11]. Assemblies with layers less than 10 nm in thickness have been fabricated by this method [6,7]. The properties of the layer are multiplied by the number of identical layers in the assembly, thereby permitting the use of conventional methods of polymer analysis for probing size-scale dependent properties as the thickness of a confined layer approaches the nanoscale.

A previous study showed that confined crystallization of polypropylene resulted in discoidal morphologies that transformed into long stacks of very short lamellae arranged in a fan-like array as the layer thickness decreased from the microscale to the nanoscale [5]. Under extreme confinement

* Corresponding author.
E-mail address: pah6@case.edu (A. Hiltner).
[1] Present address: The Dow Chemical Company, Freeport, TX 77541, USA.
[2] Present address: 3M, St. Paul, MN 55144, USA.

0032-3861/$ - see front matter © 2005 Elsevier Ltd. All rights reserved.
doi:10.1016/j.polymer.2005.01.055

Table 1
Melting behavior of HDPE/PS films (first heating)

HDPE/PS (v/v)	Film thickness (μm)	Nominal HDPE layer thickness (nm)	T_m (°C)	ΔH (J/gfilm)	ΔH (J/gHDPE)	X_c (wt% of HDPE)
100/0	305	–	134	175	175	60
50/50	279	1100	132	77	161	55
10/90	305	240	131	11.9	129	44
10/90	152	120	131	11.4	124	42
5/95	305	120	131	5.4	119	41
5/95	152	60	131	5.0	108	37
10/90	51	40	130	10.6	115	39
10/90	35	30	130	9.9	108	37
5/95	51	20	130	4.6	99	34
5/95	18	10	130	4.4	95	33
0/100	305	–	104[a]	–	–	–

[a] T_g reported for PS control film.

a second crystal population originated from the rarely observed (010) plane growth, rather than the more usual (110) growth. Decreased crystallinity was observed in polypropylene nanolayers [5], and also in confined poly-(ethylene terephthalate) nanolayers crystallized from the glassy state, [12]. In addition, highly oriented polyethylene nanolayers exhibited row-nucleated structures in which lamellae were preferentially oriented with the long axes perpendicular to the extrusion direction [4]. Loss of large scale organization, preferential orientation of chain axes, and reduced crystallinity may be general characteristics of highly confined crystallization.

Films fabricated by forced assembly are stable indefinitely under ambient conditions. However, it is inherent to the concept of forced assembly that nanolayers may not be stable when they are heated into the melt state. Thermal fluctuations at the surface of thin films are amplified by long-range dispersion forces, which lead to formation of holes and breakup of the thin film into droplets [13]. Experimental and theoretical description of film instability and the various stages of rupture, dewetting and droplet formation have focused on ultrathin films on coated substrates [14]. Imposing additional constraint by sandwiching the thin film between rigid surface layers strongly affects the instability resulting in long parallel domains rather than droplets [13,15], or even in distortion of the constraining layers [16]. Layer multiplication makes it possible to extend studies of 3-layer constrained films to consider the stability of larger assemblies of constrained polymer nanolayers.

In the present study, thin layers of high density polyethylene were coextruded between thick layers of amorphous polystyrene. The solid-state structure of the crystalline polymer was studied as the high density polyethylene layers were made thinner and confinement by the polystyrene layers approached the nanoscale. The ability to vary layer thickness also allowed us to study the nature of instabilities in highly confined thin films.

2. Experimental

2.1. Materials

Microlayer and nanolayer films with 257 alternating layers of a high density polyethylene (HDPE) and polystyrene (PS) were extruded on a laboratory scale coextrusion line at Case Western Reserve University that incorporates layer-multiplying technology [17]. The system consists of three ¾ inch (19 mm) single screw extruders with melt pumps, an ABABA coextrusion block, a series of layer multiplier elements and an exit die. The extruder temperatures were adjusted to 255 °C for HDPE and 230 °C for PS to ensure that the viscosities matched when the melts were combined in the feedblock where polymer A was PS and polymer B was HDPE. The feedblock and the multiplying die elements were maintained at 240 °C. As the melt exited the assembly of multiplying die elements, it was spread in a 6 inch (152 mm) film die and extruded onto a chill roll equipped with an air knife. The take-off speed was increased from 1.7 to 45 feet min^{-1} (0.52 to 13.7 m min^{-1}) to produce nominally 10, 5, 2, 1 and 0.7 mil (254, 127, 51, 25 and 18 μm) films with 257 alternating layers. Variations in the final film thickness and the HDPE-to-PS volumetric feed ratio produced HDPE microlayers and nanolayers of different thickness, Table 1. The nominal layer thickness was calculated using the number of layers, the feed ratio, and the film thickness. Films of HDPE and PS were extruded under the same conditions. These films served as controls for the study.

The metallocene high density polyethylene with bulk density of 0.9538 g cm^{-3}, molecular weight of 125,000 g/mol, and melt flow index of 0.8 g/10 min according to ASTM D1238 was provided by The Dow Chemical Company. The polystyrene was Dow STYRON 685D (M_w of 527 kg mol^{-1}) with bulk density of 1.0450 g cm^{-3} according to ASTM D 792 and melt flow index of 1.5 g/10 min.

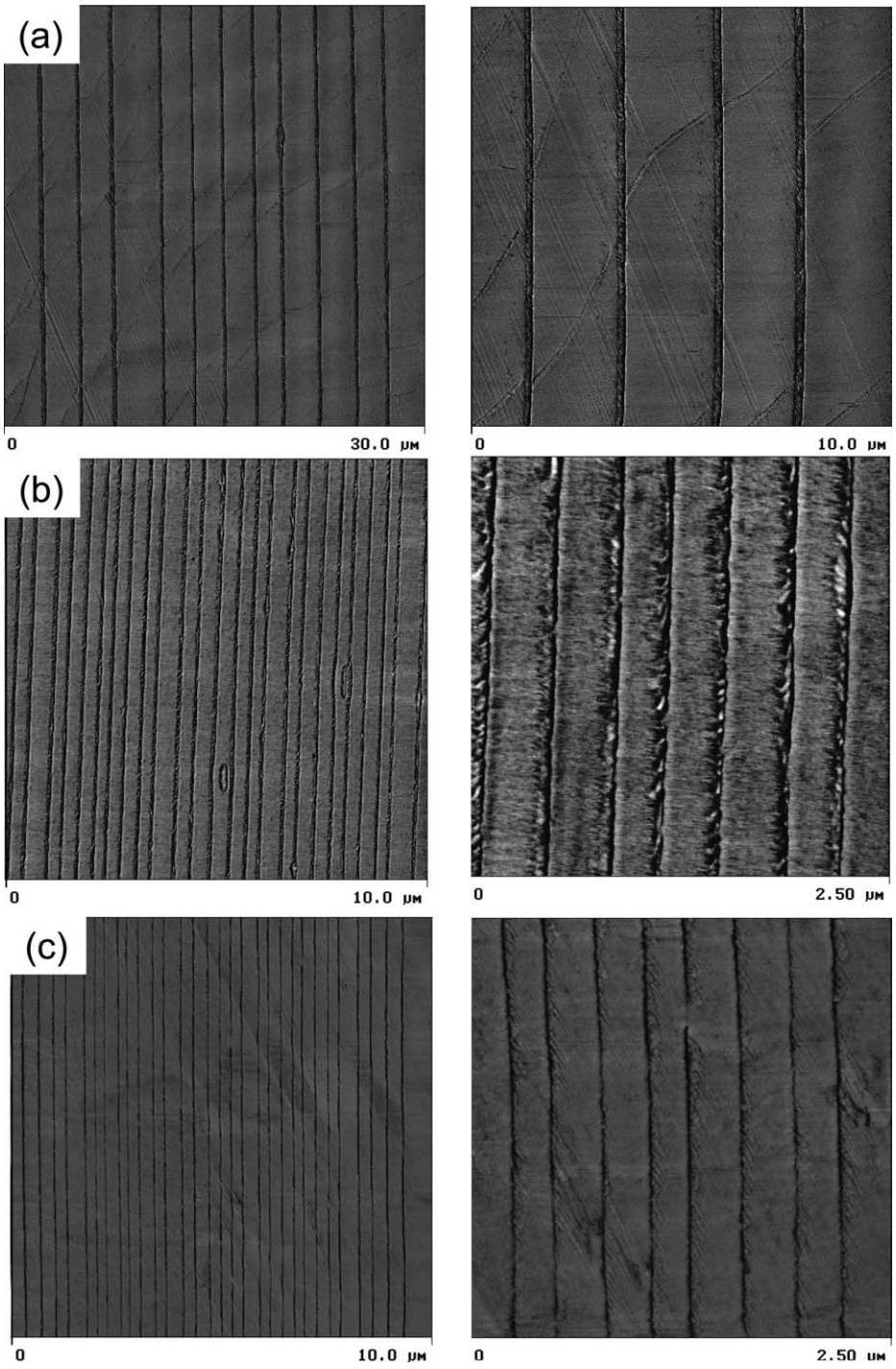

Fig. 1. AFM phase images of nanolayer films: (a) HDPE/PS 10/90 with 240 nm HDPE layers; (b) 10/90 with 40 nm layers; (c) 10/90 with 30 nm layers; (d) 5/95 with 20 nm layers; and (e) 5/95 with 10 nm layers. Two magnifications of each composition are shown.

2.2. Characterization

Layer thickness and integrity were confirmed by examining the film cross-section with atomic force microscopy (AFM). The film was embedded in epoxy (SPIChem™/SPI-PON™ 812 KIT formulation, SPI Supplies Division of Structure Probe, Inc.) and cured for 8 h at 60 °C. Cross-sections were microtomed perpendicular to the extrusion direction at −75 °C with an Ultramicrotome (MT6000-XL from RMC, Tucson, AZ) and observed directly. The AFM images were obtained in air with a commercial scanning probe microscope (Nanoscope IIIa, Digital Instruments, Santa Barbara, CA) operated in the tapping mode. The set point ratio was adjusted between 0.6 and 0.8. Height and phase images were recorded simultaneously. Measurements were performed at ambient

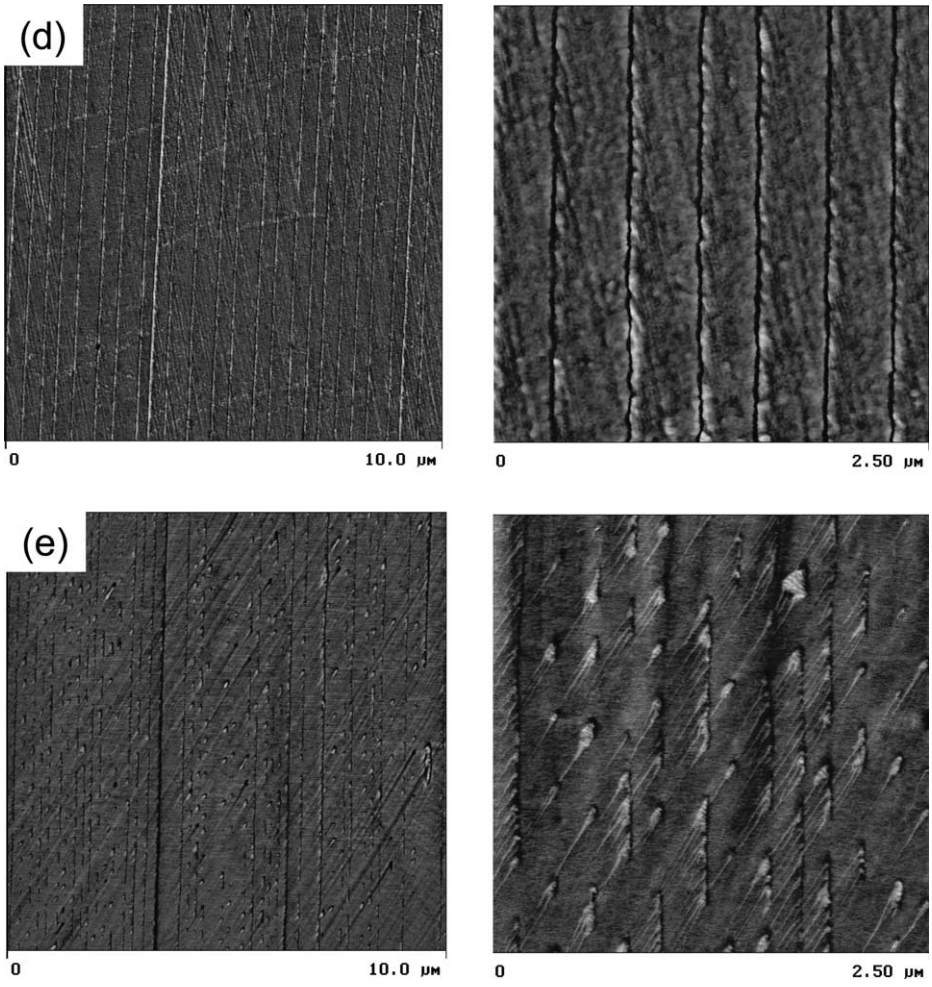

Fig. 1 (*continued*)

conditions using rectangular type Si probes with spring constant of 50 N/m and resonance frequency in the 284–362 kHz range. The tip radius was about 10 nm.

The films were peeled at liquid nitrogen temperature to expose the surface of the HDPE layer. Under these conditions the layers separated easily without deformation of the HDPE surface. The HDPE surface was imaged with the AFM tapping mode.

Heating and cooling thermograms were obtained with a Perkin Elmer Model 7 DSC. Specimens were prepared by stacking several film pieces in the DSC pan to obtain a weight of 8–12 mg. Thermograms were recorded from 30 to 200 °C with a heating/cooling rate of 10 °C min^{-1}. The first heating thermogram, the cooling thermogram, and the second heating thermogram were recorded. Crystallinity was obtained from the heat of melting using a value of 293 J/g for the heat of fusion of the polyethylene crystal [18].

The WAXS patterns (sealed-tube, fine point Cu Kα filtered source operating at 30 kV and 35 mA, Philips) were recorded with an imaging plate or film. Several film pieces were stacked and glued at the edges with isocyanate 10 s glue. The thickness of the stack was approximately 500° µm. The stacks were exposed in three orthogonal directions. For directions in the plane of the film, the stack was embedded in 5-minute epoxy and cured overnight at 23 °C. Cured specimens were sectioned perpendicular to the plane of the film to obtain 1–2 mm discs that were exposed to the X-ray beam. The stacks containing CaF_2 as an internal standard were exposed to CuKα radiation for 12 h in vacuum. Exposed imaging plates were read with a Fujifilm FDL5000 image plate reader.

Oxygen permeability at 0% relative humidity, 1 atm pressure, and 23 °C was measured with a MOCON OX-TRAN 2/20.

Thermal stability of the layers was studied by stacking film pieces to a thickness of about 350 µm. The stacks were covered with cover glasses and heated at 10 °C/min to various temperatures above the peak melting temperature of HDPE, held at temperature for 1 min, and cooled at 10 °C/min in a Rheometrics DSC under nitrogen. After thermal treatment, the stacks were embedded in epoxy and microtomed to examine the cross-section of the layers using AFM. Alternatively, the same thermal treatment was given

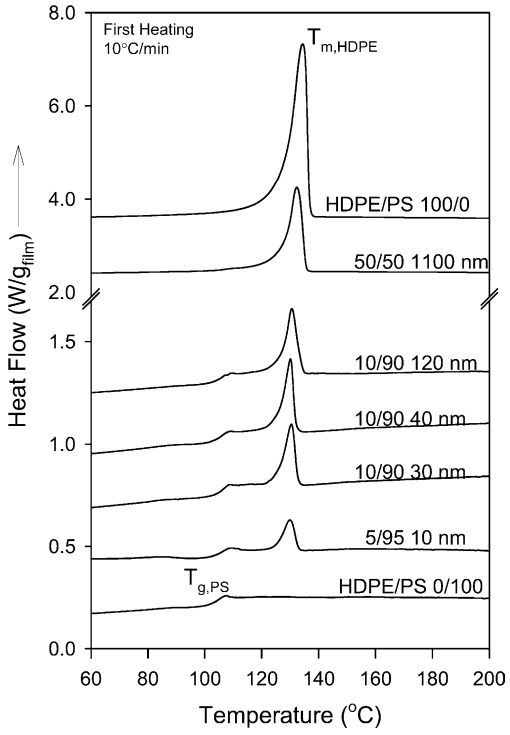

Fig. 2. Heating thermograms of HDPE/PS films. The nominal HDPE layer thickness is indicated.

to a piece of film placed between cover glasses. After thermal treatment, the film was peeled at liquid nitrogen temperature and the surface of the HDPE layer was examined using AFM.

3. Results and discussion

3.1. Layer characterization

The coextruded films were characterized by a continuous and uniform layered structure as revealed by phase images from the atomic force microscope (AFM) As examples, Fig. 1 shows partial cross-sections of films with 257 alternating layers of HDPE and PS. Thin HDPE layers were confined between thick PS layers. Differences in HDPE-to-PS composition ratio and differences in film thickness resulted in a range of HDPE layer thicknesses. The thick light bands in the AFM images corresponded to the higher modulus PS layers and the thin dark bands corresponded to the lower modulus HDPE layers, as indicated by the arrows. Continuous alternating layers were observed in films with nominal HDPE layer thickness of 20 nm or more, Fig. 1(a)–(d). When the layer thickness was forced to 10 nm, considerable layer breakup was observed, Fig. 1(e).

The layer thicknesses were measured from the section profile of the phase image. The measured HDPE layer thicknesses of the 300 μm film in Fig. 1(a) was 230 ± 30 nm, which was very close to the nominal layer thickness of 240 nm calculated from the number of layers, the feed ratio, and the film thickness. The measured thickness of the PS layers was 2230 ± 500 nm. For the 50 μm film with the same HDPE/PS 10/90 composition, shown in Fig. 1(b), the measured HDPE layer thickness of 41 ± 7 nm and the PS layer thickness of 328 ± 67 nm were very close to the calculated values of 40 and 360 nm respectively. Fig. 1(c) shows 26 ± 4 nm HDPE layers confined between 264 ± 55 nm PS layers in a 35 μm film with a HDPE/PS 10/90 composition and corresponding nominal layer thicknesses of 30 and 250 nm for HDPE and PS, respectively. Similarly, Fig. 1(d) shows a 50 μm film with a 5/95 HDPE/PS composition and nominal layer thicknesses of 20 nm for HDPE and 300 nm for PS. The measured layer thicknesses of 18 ± 3 nm for HDPE and 395 ± 96 nm for PS corresponded well to the nominal values. The thickness of the HDPE layer fragments in Fig. 1(e) was 14 ± 3 nm, which was slightly higher than the nominal thickness of 10 nm due to retraction of the fractured layers. Because films with continuous HDPE layers showed good correspondence between measured layer thickness and nominal layer thickness, the HDPE layers are identified by the nominal layer thickness.

Heating thermograms showed the glass transition of PS at 104 °C and the melting endotherm of the HDPE layers at 130–134 °C, Fig. 2. A slight reduction in the peak melting temperature with decreasing layer thickness was observed Table 1. A more significant change was a reduction in the heat of melting, which corresponded to a decrease in crystallinity from 60 to 33% for 10 nm HDPE layers.

The layers readily peeled apart when the films were cooled to cryogenic temperatures so that the exposed surfaces of HDPE layers could be imaged by AFM. Layers thicker than 100 nm contained space-filling, banded spherulitic structures with irregular boundaries, Fig. 3(a) and (b). The shape and texture of the structures as they appeared in the AFM images had no noticeable directionality with respect to the extrusion direction. As the layer thickness decreased, the diameter of the banded structures increased only slightly, from about 10 μm for 1.1 μm layers to 14 μm for 120 nm layers. This suggested that the discoids were nucleated preferentially at the HDPE/PS interfaces. In layers, bulk nucleation became insignificant and hence the size of the discoids was controlled by nucleation from the interfaces. Because the diameter was orders of magnitude larger than the layer thickness, the banded structures were flat, and were more appropriately described as discoids than as spherulites. The discoidal shape resulted from geometric confinement imposed by the PS layers that restricted spherulitic growth to 2-dimensions. The discoidal aspect-ratio (diameter to thickness) increased from 8 to 116 as the layer thickness decreased from 1.1 μm to 120 nm. Previously, discoidal structures were observed in thin polypropylene layers that were similarly confined between PS layers [5].

With decreasing layer thickness, the spacing of the

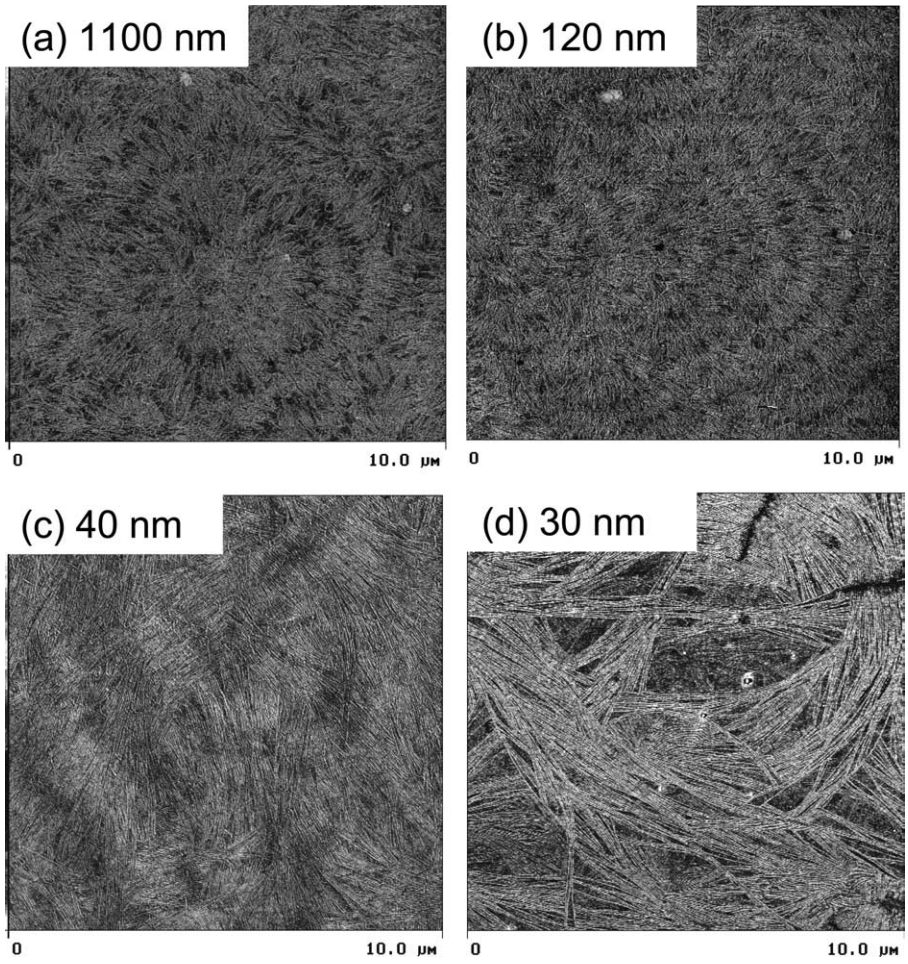

Fig. 3. AFM phase images showing the exposed HDPE surface. The nominal HDPE layer thickness is indicated.

banding pattern in HDPE discoids decreased slightly from about 1 μm for the 1.1 μm layers to 0.8 μm for the 120 nm layers. The characteristic banding pattern of spherulitic polyethylene is attributed to twisted crystallization of the lamellae, in which the chain *c*-axis spirals round the radial direction [19]. Although the discoids were formed of mostly edge-on lamellae with thickness of 20–30 nm, the 120 nm layer thickness provided sufficient space for the lamellae to twist.

As the layer thickness decreased from the microscale ($>$ 100 nm) to the nanoscale ($<$100 nm), banded discoids were no longer observed. Instead, impinging bundles of mostly edge-on lamellae comprised the morphology of HDPE nanolayers, Fig. 3(c) and (d). No preferential orientation of the bundles with respect to the extrusion direction was apparent from the AFM images. This contrasted with the highly oriented row-nucleated morphologies that were previously observed in HDPE nanolayers [4]. The difference was related to the extrusion conditions. Indeed, if the nanolayer films were extruded with a faster take-off rate and quenched more rapidly, the stacks of long lamellae were replaced with oriented shish-kebab structures.

The lamellae in nanolayers were very long, about 7 μm in length, which was approximately the same dimension as the discoids in microlayers. As a consequence, the aspect ratio (lamellar length to layer thickness) was extremely high, ranging from about 180 for 40 nm layers to about 230 for 30 nm layers. Apparently spatial confinement on the scale of tens of nanometers did not allow for twisted crystallization.

The 2-dimensional transmission diffraction patterns of HDPE microlayers and nanolayers normal to the film (ND) and parallel to the extrusion direction (ED) are compiled in Fig. 4. Patterns in the transverse direction (TD) were not discernibly different from those in the ED direction, indicating that any anisotropy in the crystal structure resulted primarily from thickness constraint rather than from the extrusion process. Reflections from the (110) and (200) planes of the orthorhombic form were clearly visible superimposed on the diffuse amorphous halo of PS. Diffraction patterns of the 1.1 μm microlayers exhibited almost isotropic rings in both ND and ED directions. However, the (200) reflection was somewhat weaker in the ND pattern than in the ED pattern, and some equatorial concentration of the (200) intensity and broad meridional concentration of the (110) intensity in the ED pattern

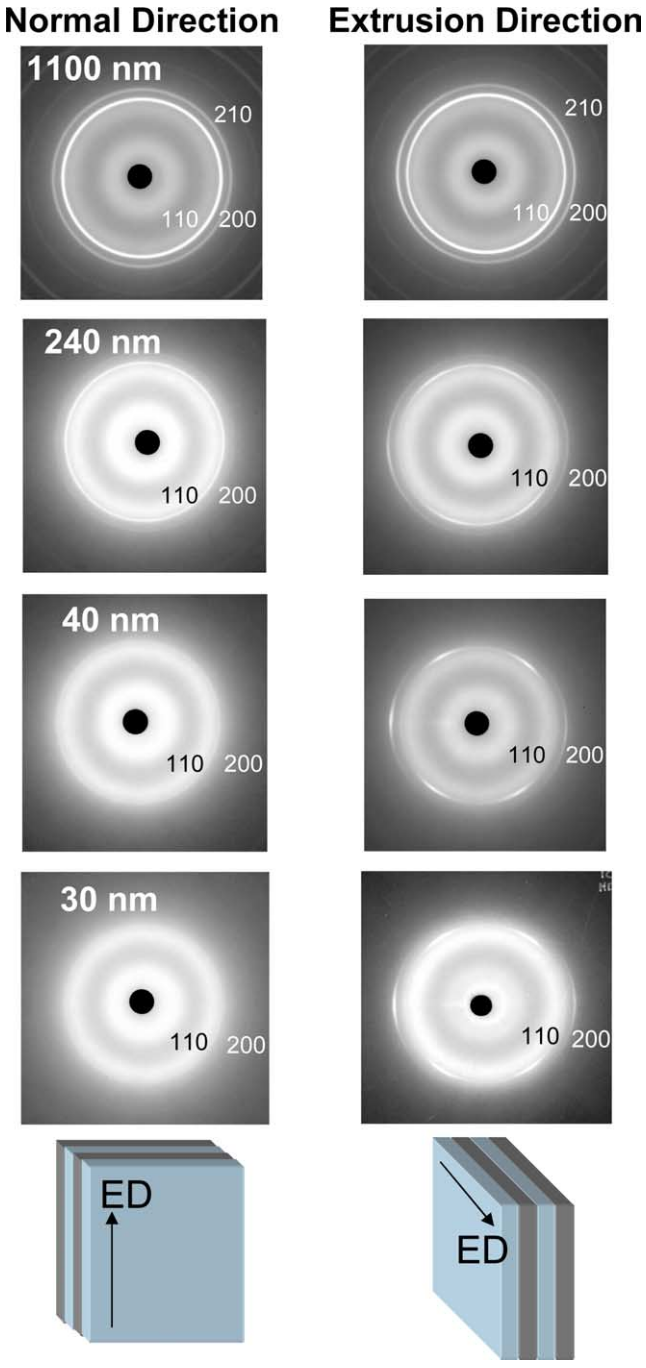

Fig. 4. WAXD patterns in the normal and extrusion directions of the HDPE/PS films. The nominal HDPE layer thickness is indicated.

suggested a certain amount of lamellar orientation with respect to the layer plane. As the layer thickness decreased to 240 nm, arcs in the ED and TD direction patterns indicated orientation in the plane of the layer. The (110) reflections appeared as arcs at approximately $+30°$ and $-30°$ with respect to the vertical. Strong equatorial intensity of the (200) reflection was consistent with preferential orientation of lamellae normal to the plane of the layer with *a*-axes normal to the layer and polymer chains parallel to the layer interface. Broadening of the (200) and (110) arcs in the ED and TD patterns of microlayers arose from lamellar twisting as observed in the AFM. The reflections sharpened as the layer thickness decreased and confinement prevented twisting of the edge-on lamellae. Similar edge-on orientation of polyethylene lamellae was achieved by epitaxial crystallization on polypropylene in extruded blend films [20].

3.2. Oxygen permeability

Gas permeability is a sensitive probe for the solid state structure of polymer nanolayers [6,7] The composite permeability P_{calc} for a layered assembly of HDPE and PS is given as:

$$P_{calc} = \left[\frac{\phi_{PE}}{P_{PE}} + \frac{1-\phi_{PE}}{P_{PS}}\right]^{-1} \quad (1)$$

where P_{PE} and P_{PS} are the permeabilities of HDPE and PS, and ϕ_{PE} is the volume fraction of HDPE. Because HDPE is less permeable to oxygen than PS, it follows that P_{calc} is very sensitive to P_{PE} if ϕ_{PE} is small. Further insight into the crystalline structure of confined HDPE layers might be revealed by the effect of layer thickness on the permeability of the polyethylene layer. The oxygen permeability of a series of films with HDPE layer thickness ranging from 1.1 μm to 20 nm was examined. Measured values of P for films that differed in composition and in layer thickness were compared with P_{calc} as determined from Eq. (1) using P_{PE} and P_{PS} measured on extruded HDPE and PS control films, Table 2. For thicker HDPE layers, on the order of 1 μm, the measured P conformed to the calculated values using Eq. (1). As the HDPE layer thickness approached the nanoscale, i.e. less than 100 nm, the measured P exceeded P_{calc}. The difference between P and the calculated permeability values (P_{calc}) increased as the layers became thinner.

The P_{calc} from Eq. (1) constituted a lower limit on P. Layer discontinuity might have caused the experimental P to be higher than expected, however AFM images confirmed continuity of HDPE layers with thickness of 20 nm or more. Alternatively, a higher value of P might have signified a structural change that resulted in increased permeability of HDPE nanolayers. From the measured P and P_{PS}, the permeability of the HDPE layer P_{PEexp} was extracted according to:

$$P_{PEexp} = \phi_{PE}\left[\frac{1}{P} - \frac{1-\phi_{PE}}{P_{PS}}\right]^{-1} \quad (2)$$

The results are plotted in Fig. 5. Permeability of thicker HDPE layers conformed to P_{PE} of the HDPE control film as indicated by the dashed line. As the HDPE layer thickness decreased to less than 100 nm, P_{PEexp} exceeded P_{PE}. The increase was as much as a factor of 3 for 20 nm thick HDPE layers, Table 2.

Permeability of a crystalline polymer is determined by

Table 2
Effect of HDPE layer thickness on oxygen permeability

HDPE/PS	HDPE layer thickness (nm)	P^a	$P_{calc}{}^a$	$P_{PEexp}{}^a$	DSC X_c (wt% of HDPE)
100/0	–	5.47±0.05	5.47	5.47	60
50/50	1100	7.90±0.07	7.96	5.4±0.1	55
10/90	120	13.0±0.1	12.5	6.6±0.1	42
5/95	120	13.8±0.1	13.5	6.8±0.6	41
5/95	60	14.1±0.1	13.5	8.5±1.1	37
5/95	20	14.6±0.1	13.5	14.6±2.1	34
0/100	–	14.6±0.2	14.6	–	–

[a] P, P_{calc}, P_{PEexp}-Permeability, cc(STP) cm m^{-2} day^{-1} atm^{-1}.

the volume fraction of permeable amorphous phase [21,22], and is also affected by the crystalline morphology, which impacts the tortuosity of the diffusion pathway [23,24]. It seems reasonable that both lower crystallinity and edge-on orientation of lamellae contributed to increased oxygen permeability of highly confined HDPE nanolayers.

3.3. Fractionated crystallization

Cooling the films from the melt produced the DSC thermograms in Fig. 6. Films with HDPE layer thickness of 120 nm or more exhibited a single crystallization exotherm at the same temperature as the HDPE extruded control film, T_{c1} at about 116 °C. Films with HDPE layer thickness less than 100 nm exhibited two crystallization exotherms, the normal one at 116 °C and another, T_{c2} at about 80 °C, with very large supercooling. As the layer thickness decreased, the enthalpy associated with T_{c1} gradually decreased and the enthalpy associated with T_{c2} correspondingly increased until primarily crystallization at T_{c2} was observed for nanolayers 10 nm thick.

The presence of more than one crystallization exotherm is known as fractionated crystallization [25,26]. The lowest temperature exotherm with the largest supercooling is usually associated with homogeneous nucleation [25–32]. For polyethylene, the lowest crystallization temperature reported for homogeneous nucleation is around 70 °C [32]. Therefore, the crystallization peak at about 116 °C was attributed to heterogeneous nucleation and the one at about 80 °C to homogeneous nucleation. Peak crystallization temperatures and the corresponding crystallization enthalpies for heterogeneous and homogeneous crystallization are summarized in Table 3. Enthalpy associated with the small amount of crystallization at temperatures intermediate between T_{c1} and T_{c2} was included with ΔH_{c1}.

The peak crystallization temperatures either did not change (T_{c1}) or changed by only a few degrees (T_{c2}) with layer thickness. However, the amount of homogeneously nucleated HDPE strongly depended on the nominal layer thickness. Whereas a small amount of HDPE in 120 nm layers crystallized by homogeneous nucleation, in contrast HDPE in 10 nm layers crystallized primarily by homogeneous nucleation. The decrease in total crystallization enthalpy ΔH_c with nominal layer thickness paralleled the trend observed in the initial melting enthalpy of the HDPE

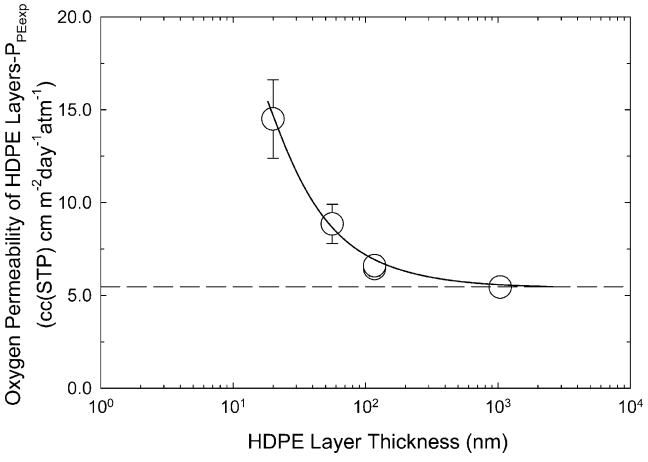

Fig. 5. Effect of layer thickness on the oxygen permeability of the HDPE layer.

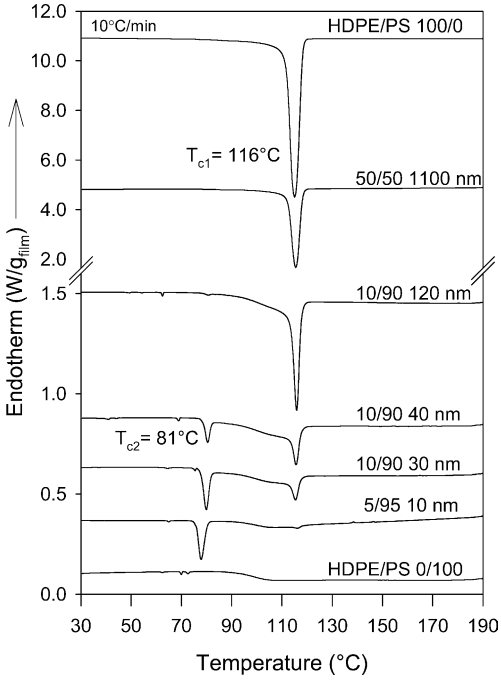

Fig. 6. Cooling thermograms of HDPE/PS films. The nominal HDPE layer thickness is indicated.

Table 3
Thermal behavior of HDPE/PS nanolayered films

HDPE/PS (v/v)	Nominal HDPE layer thickness (nm)	Crystallization							Melting (2nd Heating)		
		T_{c1} (°C)	ΔH_1 (J/gHDPE)	X_{c1} (wt%)	T_{c2} (°C)	ΔH_2 (J/gHDPE)	X_{c2} (wt%)	ΔH_{Total} (J/gHDPE)	X_{cTotal} (wt%)	T_m (°C)	ΔH_m (J/gHDPE)	X_m (wt%)
100/0	–	115	195	67	–	–	–	195	67	136	197	67
50/50	1100	115	181	62	–	–	–	181	61	135	176	60
10/90	240	116	149	51	–	–	–	149	51	133	154	53
10/90	120	116	143	49	81	1.4	0.5	145	51	133	150	51
5/95	120	117	136	46	81	0.7	0.2	137	47	133	138	47
5/95	60	116	123	42	81	8.6	2.9	131	45	132	128	44
10/90	40	115	105	36	81	21	7.3	126	44	131	129	44
10/90	30	115	76	26	80	37	13	113	39	131	118	40
5/95	20	116	44	15	80	59	20	103	35	132	102	35
5/95	10	116	29	10	78	75	26	105	36	131	100	34

layers (see Table 1). Regardless of whether the HDPE crystallized by homogeneous or heterogeneous nucleation, a single melting endotherm was observed in the subsequent heating thermogram. Close correspondence was observed between the crystallization enthalpy ΔH_c and the subsequent melting enthalpy ΔH_m, Table 3.

Fractionated crystallization has been observed in polymer droplets dispersed in a low molecular weight medium, [27,28,30,33] in polymer blends, [25,26,29,31,32] and in block copolymers [34–36]. For fractionated crystallization to occur, the polymer melt must be dispersed finely enough that the number of droplets is significantly greater than the number of heterogeneities that are active at low supercoolings [33]. As a result, most of the droplets contain either less efficient heterogeneities or no heterogeneities at all.

Although homogeneously nucleated droplets are usually very small, even droplets as large as 20 μm can be homogeneously nucleated provided that the number of particles in the subdivided bulk is larger than the number of active heterogeneities [37,38]. To date, the smallest droplet size that has been reported in a polymer blend exhibiting fractionated crystallization is 100 nm [35].

The droplets responsible for fractionated crystallization resulted from instability and breakup of the nanolayers when they were taken into the melt. Indeed, one method for preparing assemblies of polymer droplets small enough to exhibit homogeneous nucleation utilizes instability and breakup of thin polymer films [38]. Cross-sections of films that had been heated to 200 °C, which was 70 °C above the peak melting temperature of HDPE, showed that melting transformed the confined HDPE nanolayers into HDPE particles dispersed in a PS matrix, Fig. 7. The particle diameter depended on the initial layer thickness. Microlayers 120 nm thick produced droplets with an average diameter of 2 μm, whereas breakup of nanolayers 10 nm thick formed droplets with an average diameter of 140 nm. Apparently the number of droplets produced by breakup of 120 nm microlayers was small enough that each droplet contained at least one heterogeneity, because only the single crystallization exotherm at T_{c1} was observed, Fig. 7. In contrast, the number of droplets formed by breakup of the 10 nm nanolayers was large enough that the majority did not contain an active heterogeneity. Observation of droplets as small as 10 nm suggested that controlled nanolayer breakup could be used as a method for creating dispersions of polymer nanodroplets.

3.4. Layer breakup

The process by which continuous HDPE layers broke up into droplets was revealed by heating films with HDPE layer thickness of 40 nm to various temperatures above the peak melting temperature of HDPE. Films were heated at 10 °C/min to the temperatures superimposed on the heating thermogram in Fig. 8, held at temperature for 1 min and cooled at 10 °C/min. After thermal treatment, the films were

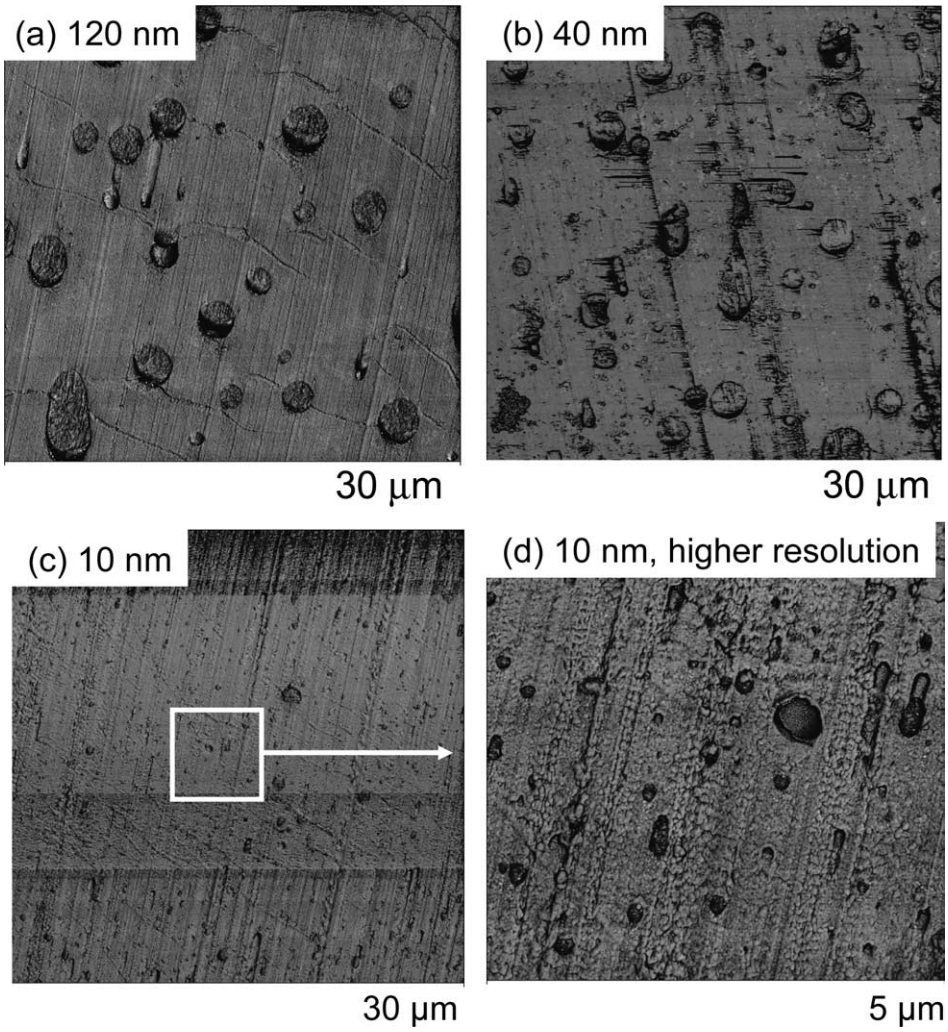

Fig. 7. AFM phase images showing the cross-section of HDPE/PS films after heating to 200 °C. The nominal HDPE layer thickness is indicated.

examined in cross-section. Additionally, the films were peeled apart and the surface of the exposed HDPE layer was examined.

The cross-sectional AFM phase images of 40 nm HDPE layers at different stages of breakup are shown in Fig. 8. The first indication of instability in the continuous and uniform HDPE layers occurred after the film was heated to 138 °C, slightly above the HDPE melting peak at 134 °C. Discontinuities in the HDPE layers indicated formation of holes. Rupture was accompanied by layer contraction and thickening, which became progressively more pronounced as the temperature increased to 144 and 154 °C. Evidence of the continuous uniform layering of the original film was largely removed by heating to 174 °C leaving a dispersion of thick layer remnants and droplets about 1 µm in diameter. After heating to 200 °C, the HDPE was mostly in the form of droplets. The droplet diameter increased to several microns due to droplet coalescence. The breakup process is summarized by plotting the dimensions of each of the morphological features in Fig. 9.

Evidence of irregularly shaped holes was visible on the exposed surface of an HDPE layer after heating to 138 °C, Fig. 10(a). When holes formed in the HDPE layer, PS layers on either side fused. As the film was peeled, brittle fracture of the fused PS appeared as the rough surface texture on the phase image and irregular protrusions on the height image. The remaining HDPE layer recrystallized with the original texture characterized by bundles of long, edge-on lamellae. These holes appeared as layer discontinuities in cross-sections of the film heated to 138 °C (see Fig. 8), and constituted the first indication of instability. Heating to 174 °C resulted in larger holes, as shown in Fig. 10(b). The PS fracture surface contained at least one 1 µm HDPE droplet (arrow) that formed from HDPE layer breakup. Thickening of the HDPE layer around the hole resulted in recrystallization as short, randomly oriented lamellae.

It can be imagined that as the temperature increased into the melting range of HDPE, the continuous HDPE layer became fluid enough for thermal fluctuations to cause rupture. When this occurred, the layer readily contracted from the rupture site because the PS layers were above the glass transition temperature and no longer constraining on

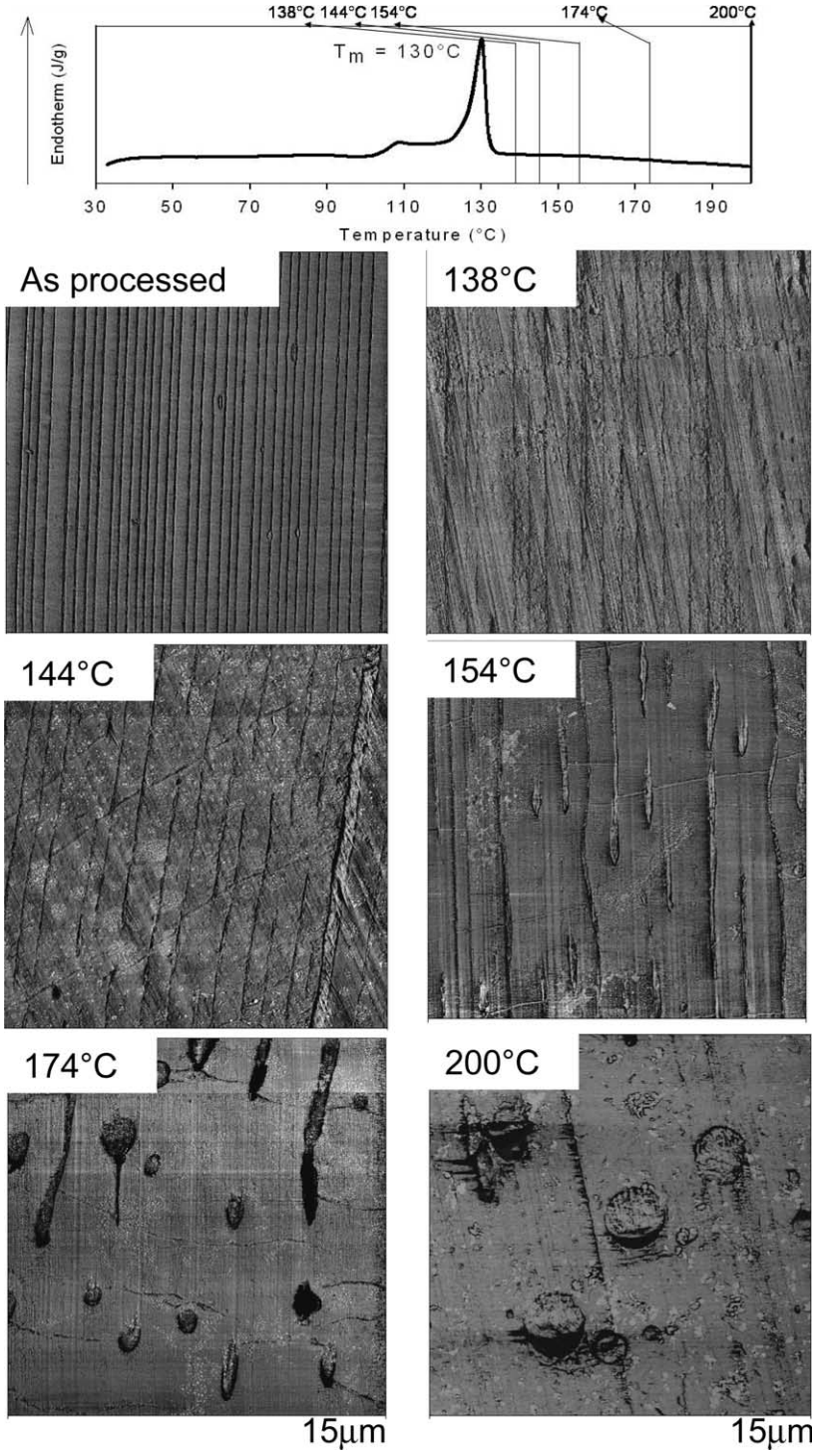

Fig. 8. AFM phase images showing the cross-section of HDPE/PS films after heating to the temperature indicated. The nominal HDPE layer thickness was 40 nm.

the HDPE layers. Consequently, the hole expanded rapidly. As the isolated holes grew, they encountered other holes, coalesced, and left a layer remnant that transformed into a droplet shape due to surface tension effects. The markedly smaller particles of the 10 nm film might have formed differently. The layers of this film broke up during processing. Relaxation of individual layer fragments would have produced droplets of the size observed in Fig. 7(d).

4. Conclusions

This study examined crystallization and thermal stability

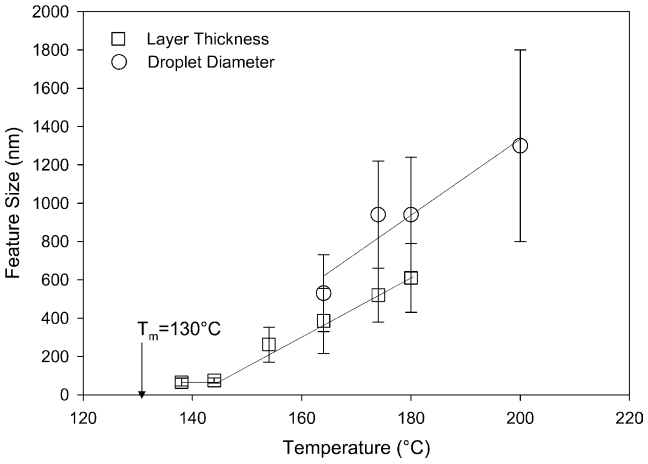

Fig. 9. Dimension of features observed during breakup of 40 nm HDPE layers.

of HDPE when confined to very thin layers. Films with hundreds of thin HDPE layers separated by thicker amorphous PS layers were fabricated by layer-multiplying coextrusion. The thickness of continuous HDPE layers varied from 1.1 μm to 20 nm. Characterization of the films by conventional methods of polymer analysis revealed changes in the structure and properties of the HDPE layers as the thickness decreased from the microscale (>100 nm) to the nanoscale (<100 nm). Crystallization preserved the normal orthorhombic form. Confinement at the microscale imposed a layer thickness that was less than the spherulite dimension. Under this condition, lamellae organized as flattened spherulites, or discoids. Although the banded discoids formed of mostly edge-on lamellae, microscale confinement provided sufficient space for the lamellae to twist. Nanoscale confinement resulted in crystallization as

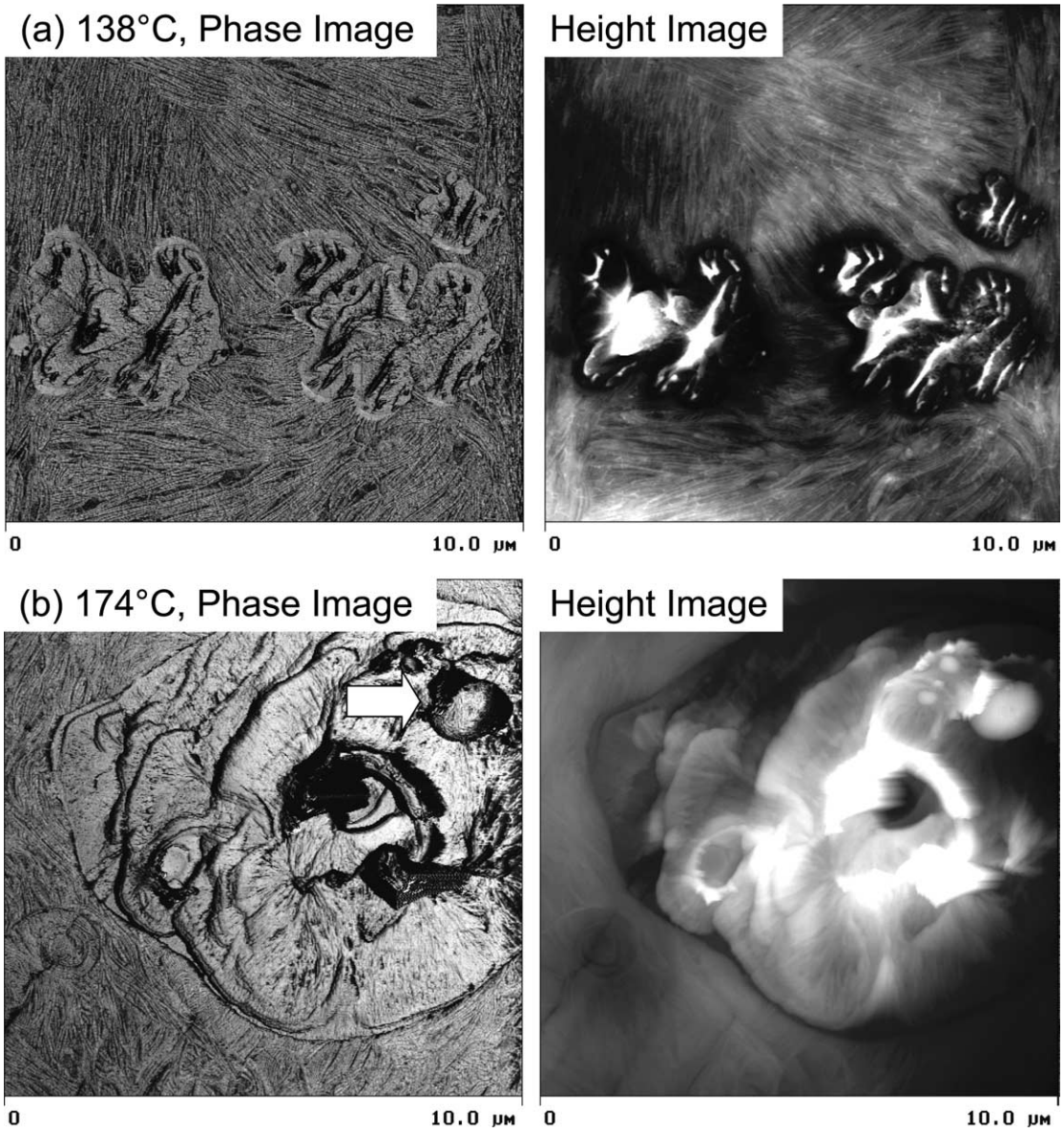

Fig. 10. AFM phase images and corresponding height images showing the exposed HDPE surface after heating to the temperature indicated. The nominal HDPE layer thickness was 40 nm.

long bundles of edge-on lamellae. As the HDPE layers became thinner, the crystallinity decreased from about 60% to almost 30%. Changes in crystallinity and crystalline morphology were responsible for an increase in oxygen permeability of the HDPE layer.

It is inherent to the concept of forced assembly that nanolayers may not be stable when they are heated into the melt state. Heating films above the melting temperature of HDPE resulted in fractionated crystallization as indicated by two crystallization exotherms in thermograms: one at the normal crystallization temperature near 116 °C and the other near 80 °C. The lower temperature exotherm was identified with homogeneous nucleation. The droplets responsible for fractionated crystallization resulted from instability and breakup of the layers when they were taken into the melt. Nanodroplets formed by melting 10 nm layers were numerous enough that the majority did not contain an active heterogeneity and crystallization occurred primarily by homogeneous nucleation.

Acknowledgements

This research was generously supported by the National Science Foundation Grant DMR-0349436, Polymer Program. T.E. Bernal-Lara gratefully acknowledges the support received from Grupo CYDSA, S.A. de C.V. and CONACYT (Consejo Nacional de Ciencia y Tecnología).

References

[1] Balsamo V, Stadler R. Macromolecules 1999;32:3994–9.
[2] Loo Y-L, Register RA, Ryan AJ, Dee GT. Macromolecules 2001;34:8968–77.
[3] Michler GH, Adhikari R, Lebek W, Goerlitz S, Weidisch R, Knoll K. J Appl Polym Sci 2002;85:683–700.
[4] Pan SJ, Im J, Hill MJ, Keller A, Hiltner A, Baer E. J Polym Sci, Part B: Polym Phys 1990;28:1105–19.
[5] Jin Y, Rogunova M, Hiltner A, Baer E, Nowacki R, Galeski A, et al. J Polym Sci, Part B: Polym Phys 2004;42:3380–96.
[6] Liu RYF, Jin Y, Hiltner A, Baer E. Macromol Rapid Commun 2003;24:943–8.
[7] Liu RYF, Bernal-Lara TE, Hiltner A, Baer E. Macromolecules 2004;37:6972–9.
[8] Whitesides GM, Grzybowski B. Science 2002;295:2418–21.
[9] Baer E, Hiltner A, Keith HD. Science 1987;235:1015–22.
[10] Kerns J, Hsieh A, Hiltner A, Baer E. J Appl Polym Sci 2000;77:1545–57.
[11] Mueller C, Topolkaraev V, Soerens D, Hiltner A, Baer E. J Appl Polym Sci 2000;78:816–28.
[12] Baltá Calleja F, Ania F, Puente Orench I, Baer E, Hiltner A, Bernal-Lara TE, Funari S. Prog Colloid Polym Sci, (in press).
[13] Dutcher JR, Dalnoki-Veress K, Nickel BG, Roth CB. Macromol Symp 2000;159:143–50.
[14] Sharma A, Reiter G. J Colloid Interface Sci 1996;178:383–99.
[15] Dalnoki-Veress K, Nickel BG, Dutcher JR. Phys Rev Lett 1999;82:1486–9.
[16] David MO, Reiter G, Sitthai T, Schultz J. Langmuir 1998;14:5667–72.
[17] Mueller C, Kerns J, Ebeling T, Nazarenko S, Hiltner A, Baer E. Microlayer coextrusion: processing and applications. In: Coates PD, editor. Polymer processing engineering 97. London: The Institute of Materials; 1997. p. 137–57.
[18] Wunderlich B. Macromolecular physics. vol.3. New York: Academic Press; 1980 pp. 58.
[19] Bassett DC. Principles of polymer morphology. Cambridge: Cambridge University Press; 1981 p. 22.
[20] Chang AC, Tau L, Hiltner A, Baer E. Polymer 2002;43:4923–33.
[21] Sekelik DJ, Stepanov EV, Nazarenko S, Schiraldi D, Hiltner A, Baer E. J Polym Sci, Part B: Polym Phys 1999;37:847–57.
[22] Polyakova A, Stepanov EV, Sekelik D, Schiraldi DA, Hiltner A, Baer E. J Polym Sci, Part B: Polym Phys 2001;39:1911–9.
[23] Hu YS, Liu RYF, Zhang LQ, Rogunova M, Schiraldi DA, Nazarenko S, et al. Macromolecules 2002;35:7326–37.
[24] Hu YS, Liu RYF, Rogunova M, Schiraldi DA, Nazarenko S, Hiltner A, et al. J Polym Sci, Part B: Polym Phys 2002;40:2489–503.
[25] Ghijsels A, Groesbeek N, Yip CW. Polymer 1982;23:1913–6.
[26] Morales RA, Arnal ML, Müller AJ. Polym Bull 1995;35:379–86.
[27] Koutsky JA, Walton AG, Baer E. J Appl Phys 1967;38:1832–9.
[28] Ross GS, Frolen LJ. J Res Nat Bur Stand-A 1975;794(6):701–11.
[29] Santana OO, Müller AJ. Polym Bull 1994;32:471–7.
[30] Barham PJ, Jarvis DA, Keller A. J Polym Sci, Part B: Polym Phys 1982;20:1733–48.
[31] Arnal ML, Matos ME, Morales RA, Santana OO, Müller AJ. Macromol Chem Phys 1998;199:2275–88.
[32] Arnal ML, Müller AJ. Macromol Chem Phys 1999;200:2559–76.
[33] Cormia RL, Price FP, Turnbull D. J Chem Phys 1962;37:1333–40.
[34] Chen HL, Wu J, Lin T, Lin JS. Macromolecules 2001;34:6936–44.
[35] Müller AJ, Balsamo V, Arnal ML, Jakob T, Schmalz H, Abetz V. Macromolecules 2002;35:3048–58.
[36] Loo YL, Register RA, Ryan AJ. Phys Rev Lett 2000;84:4120–3.
[37] Massa MV, Carvalho JL, Dalnoki-Veress K. Eur Phys J E 2003;12:111–7.
[38] Massa MV, Dalnoki-Veress K. Phys Rev Lett 2004;92:255509.